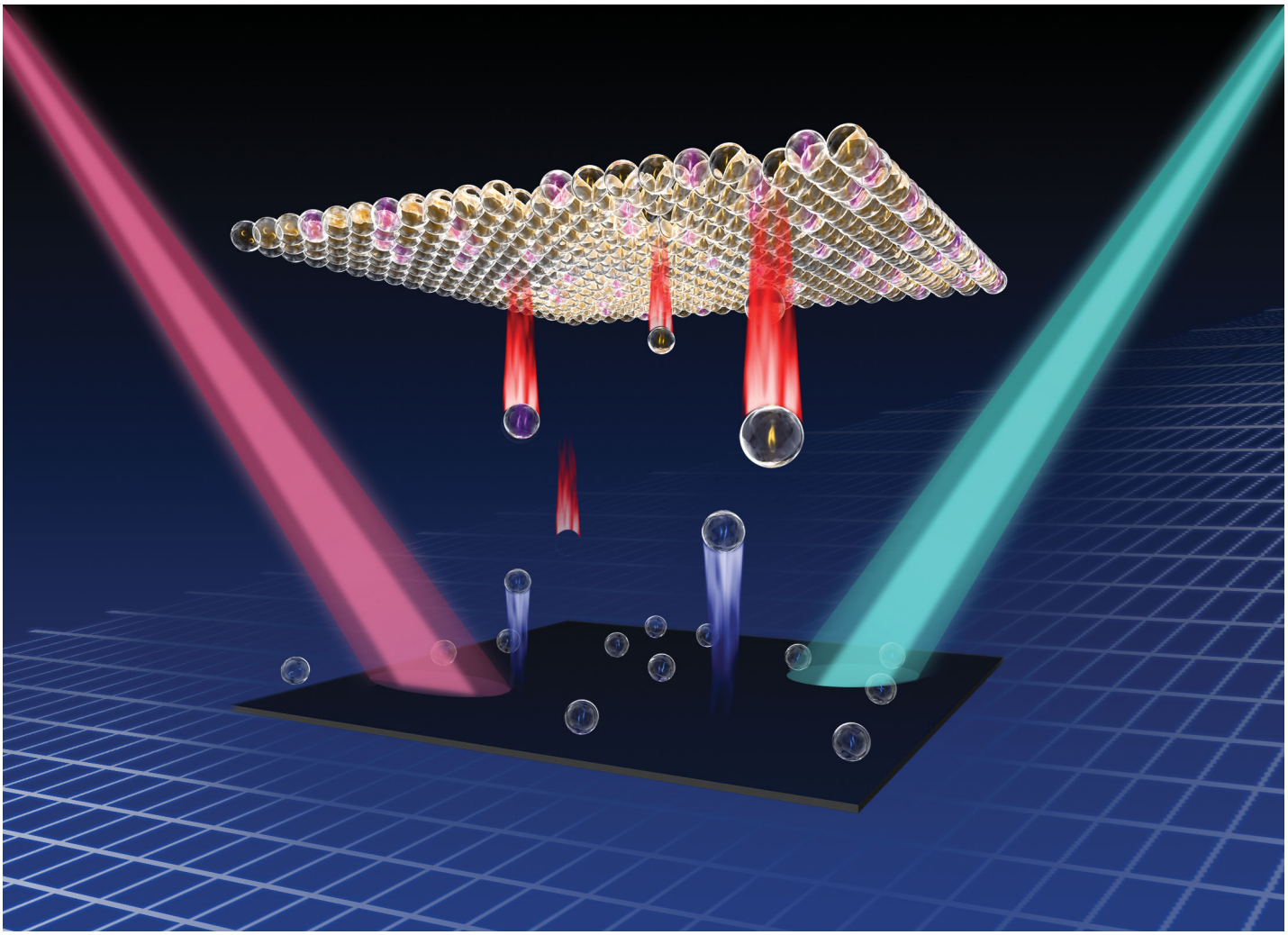

Showcasing research from the Key Laboratory of Optoelectronic Devices and Systems of Ministry of Education and Guangdong Province, College of Optoelectronic Engineering, Shenzhen University, China and the Department of Applied Physics and Materials Research Center, The Hong Kong Polytechnic University, Kowloon, China

Technique and model for modifying the saturable absorption (SA) properties of 2D nanofilms by considering interband exciton recombination

By considering interband exciton recombination, two-dimensional nanofilms saturable absorption properties under excitation by laser pulses with various durations in the fs, ps and ns ranges, are investigated theoretically and experimentally.

As featured in:

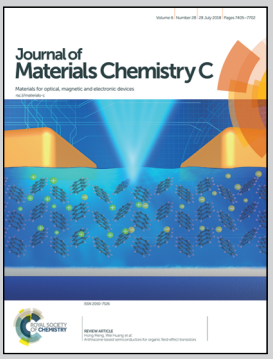

See Yuen Hong Tsang, Qiao Wen *et al.*, *J. Mater. Chem. C*, 2018, **6**, 7501.

ROYAL SOCIETY OF CHEMISTRY

rsc.li/materials-c

Registered charity number: 207890

Journal of Materials Chemistry C

PAPER

View Article Online
View Journal | View Issue

Cite this: J. Mater. Chem. C, 2018, 6, 7501

Technique and model for modifying the saturable absorption (SA) properties of 2D nanofilms by considering interband exciton recombination†

Guowen Liang,‡[a] Longhui Zeng,‡[b] Yuen Hong Tsang,*[b] Lili Tao,[b] Chun Yin Tang,[b] Ping Kwong Cheng,[b] Hui Long,[b] Xin Liu,[a] Ji Li,[a] Junle Qu [a] and Qiao Wen *[a]

Received 30th January 2018,
Accepted 11th April 2018

DOI: 10.1039/c8tc00498f

rsc.li/materials-c

In this study, we have successfully demonstrated a method of greatly modifying the nonlinear saturable absorption (SA) properties of WS2 nanofilms by controlling their thickness and morphology *via* magnetron sputtering deposition times. The nonlinear SA properties of these nanofilms were also investigated systematically under excitation by laser pulses with various durations in the fs, ps and ns ranges, and prominent ultrafast SA parameters were demonstrated for different pulse durations in the fs, ps and ns ranges. A pulse width-dependent theoretical model of SA that considers the effects of interband exciton recombination has now been proposed for the first time. Two analytical expressions for calculating the variation of key SA parameters (the onset fluence F_{on} and the modulation depth ΔT) with the excitation laser pulse width have been derived and experimentally verified. The theoretical model and analytical expressions have great value for understanding and interpreting the variation of the SA behaviors of 2D nanofilms in the fs, ps and ns regions, and for the developments of ultrafast lasers and nanosecond lasers based on 2D materials. These studies open up exciting avenues for engineering the SA properties of 2D nanofilms for a wide range of laser photonic devices and applications.

1 Introduction

Two-dimensional (2D) layered materials are currently attracting great research interest and attention from the optics, laser, photonics and optoelectronics research communities for their potential to bring revolutionary changes to these fields. 2D materials exhibit exceptional electrical and optical properties compared to their bulk forms due to the quantum confinement perpendicular to the 2D plane.[1] Soon after the discovery of graphene in 2004,[2,3] scientists demonstrated advanced electric and photonic applications such as photodetectors,[4–8] light-emitting diodes,[9] phototransistors,[10,11] solar cells,[12] optical waveguides,[13] and ultrafast lasers[14] by using graphene. However, the zero-bandgap nature and low layer optical absorption of graphene limits its application in the field of photonics and nonlinear optics. Therefore, the research focus has been extended to other 2D materials[15–18] with natural bandgaps. In the past few years, the emergence of 2D transition metal dichalcogenides (TMDs), *e.g.*, MX_2 (M = Mo, W; X = S, Se), has attracted increasing attention because of their wide bandgap range from near-infrared to the visible region[19] and their unique and favorable electrical, optical, thermal and mechanical properties.[20] Layered TMDs are a new class of functional materials and have been used extensively in various applications such as nanoelectronics,[21] solar cells,[22] photodetectors,[23] nonlinear optics[24–26] photocatalysis[27] and energy storage.[28] Molybdenum disulfide (MoS_2) is the most studied member of the TMD family for nonlinear optical applications,[29–31] and very recently, the novel tungsten disulfide (WS_2) began to receive significant attention because of its tunable bandgap arising from indirect-to-direct bandgap transition with a decreasing number of layers, high carrier mobility and strong spin–orbit coupling due to its asymmetric structure and favorable photonic properties.[32,33] WS_2 exhibits strong nonlinear optical limiting properties and is tunable by adjustment of the size and thickness.[24] Therefore, the saturable absorption (SA) properties of these novel 2D materials are an important research topic, as the mainstream saturable absorbers used for Q-switching and mode locking, *e.g.*, doped crystals and SESAMs, still have some limitations such as narrow operation wavebands, limited response times, high cost, and complex fabrication processes.[34,35] A previous study confirmed that WS_2 exhibits strong SA properties and an

[a] Key Laboratory of Optoelectronic Devices and Systems of Ministry of Education and Guangdong Province, College of Optoelectronic Engineering, Shenzhen University, Shenzhen 518060, China. E-mail: wenqiao@szu.edu.cn
[b] Department of Applied Physics and Materials Research Center, The Hong Kong Polytechnic University, Kowloon, Hong Kong, China. E-mail: yuen.tsang@polyu.edu.hk

† Electronic supplementary information (ESI) available. See DOI: 10.1039/c8tc00498f
‡ These authors contributed equally to this work. Both institutes contributed equally to this work.

ultrahigh optical damage threshold with a broad operational wavelength range from the visible range[36–38] up to the mid infrared range;[39,40] therefore, Q-switching[32,34,36–38,40–45] and mode locking[32,35,39,46–48] laser pulses can be generated by utilizing WS_2 as a saturable absorber in various laser systems. The fabrication of WS_2 film is relatively simple and low cost compared with that of the mainstream saturable absorbers used in commercial pulsed laser products.

Additionally, WS_2 and other new TMDs, can be widely used in other photonic device applications, *e.g.*, optical communications and optical computing.[49] The performance of such devices is largely dependent upon the nonlinear optical parameters of the 2D SA materials, and therefore, tuning and characterizing the parameters of 2D SA properties has become a highly important research topic for various nonlinear optical applications.[50–53] For the above reasons, this research aims to examine the SA properties of TMDs with different film thicknesses and structures for different pulse durations and lifetimes.

In this study, polycrystalline WS_2 film samples with various thicknesses were fabricated by the magnetron sputtering deposition method because of its high production speed and scalability compared with the CVD method. The WS_2 film thickness and structure depend on the sputtering time. The SA properties of the WS_2 films were then investigated under excitation by an 800 nm laser pulse with various pulse widths (100 fs, 10 ps, 200 ps, 10 ns) but the same pulse energy by using an open aperture (OA) Z-scan method. A theoretical model showing the relationship between the key SA parameters and the excitation pulse width, considering the effects of interband exciton recombination, was developed for the first time, and analytical expressions for the variation of these key SA parameters with the pulse width were deduced. The expressions were experimentally verified by Z-scan experiments. These analytical expressions provide a new way to estimate the SA parameters of any TMD film for various ultrafast pulse duration ranges. These studies will allow us to gain deeper understanding for engineering the nonlinear SA properties of the 2D materials and will significantly benefit the development of 2D materials for a wide range of nonlinear optical applications, including passive mode-lockers, passive Q-switchers, optical switches, ultrafast pulse shaping devices, and optical signal processing devices used in optical communication systems and optical computing.

2 Sample preparation and characteristics

The WS_2 samples used for this experiment were fabricated by the magnetron sputtering of WS_2 onto a clean quartz substrate for various periods of time (1 min, 3 min and 5 min) to control its film thickness followed by post-annealing. WS_2 precursor films were first produced through sputtering by using a sintered WS_2 disk as the target. The post annealing process was then conducted to enhance the crystallinity of the WS_2 film and replenish the S contents in the WS_2. Fig. 1(a) displays photographs of post-annealed polycrystalline WS_2 film on a quartz substrate,

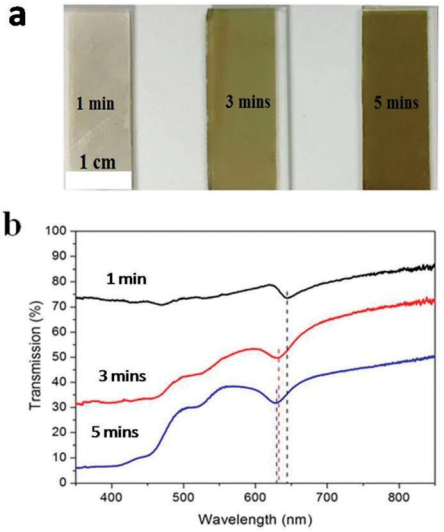

Fig. 1 (a) Photographs and (b) transmission spectra of WS_2 films fabricated with different magnetron sputtering times.

showing a characteristic change from dark gray to yellow and yellowish green. The transmittance spectra of WS_2 films with different thicknesses are presented in Fig. 1(b), which clearly shows absorption characteristic peaks located between 600 and 650 nm. The characteristic absorption peaks of WS_2 films fabricated with different sputtering times (1 min, 3 min, and 5 min) were located at 644.5 nm, 632 nm and 629 nm, respectively. The differences in peak position between samples indicate that polycrystalline WS_2 films with different thicknesses and morphologies can be fabricated by controlling the magnetron sputtering time. The transmittance spectra showed that the peak position of the WS_2 film shifts to shorter wavelengths as the sputtering time increases.[54]

The surface topography of the WS_2 films was investigated by atomic force microscopy (AFM) measurement as shown in Fig. 2(a–c), which revealed that all the WS_2 films were continuous. The corresponding section height profiles of the WS_2 samples were measured and are shown in Fig. 2(d–f). The measured film thicknesses were 8.85 nm, 15.7 nm, and 27.7 nm for the 1 min, 3 min and 5 min WS_2 films, respectively.

Raman spectroscopy is a powerful tool for the investigation of the crystal structures and layer numbers of the WS_2 films. Therefore, Raman mappings of all the WS_2 films samples were recorded and are shown in Fig. 3. As expected, the WS_2 samples show two strong signals due to the in-plane vibration E^1_{2g} of the tungsten and sulfur atoms and the out-of-plane vibration A_{1g} of the sulfur atoms. Both dominant Raman modes with wave numbers of approximately 350 cm^{-1} and 420 cm^{-1}, respectively, can be identified in Fig. 3, which is in good agreement with the results found in previous reports.[55] According to previous reports, the frequency difference between the E^1_{2g} and A_{1g} modes of TMDs, $\Delta\omega$, is dependent on the average layer number.[56] In general, $\Delta\omega$ decreases as the average layer number decreases.[57] The measured $\Delta\omega$ values of the 1 min, 3 min and 5 min WS_2 samples were 65.7 cm^{-1}, 65 cm^{-1} and 64.2 cm^{-1} respectively. These results

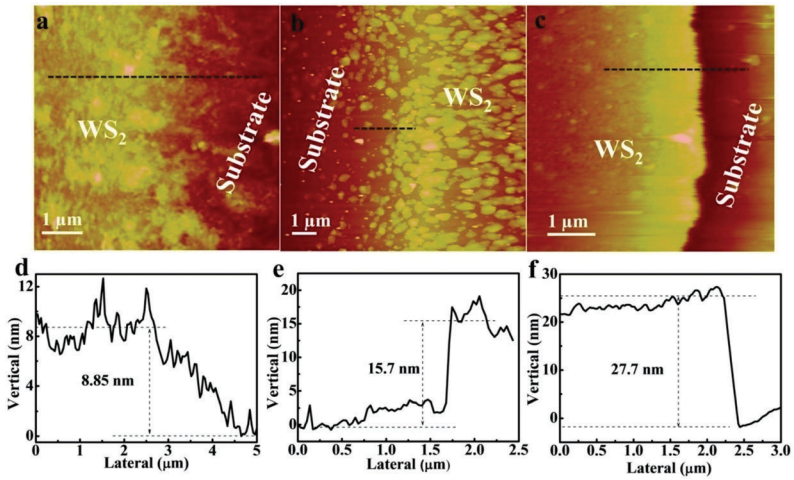

Fig. 2 (a–c) AFM images of WS_2 films; (d–f) height profiles of WS_2 films obtained with 1 min, 3 min and 5 min sputtering time, respectively.

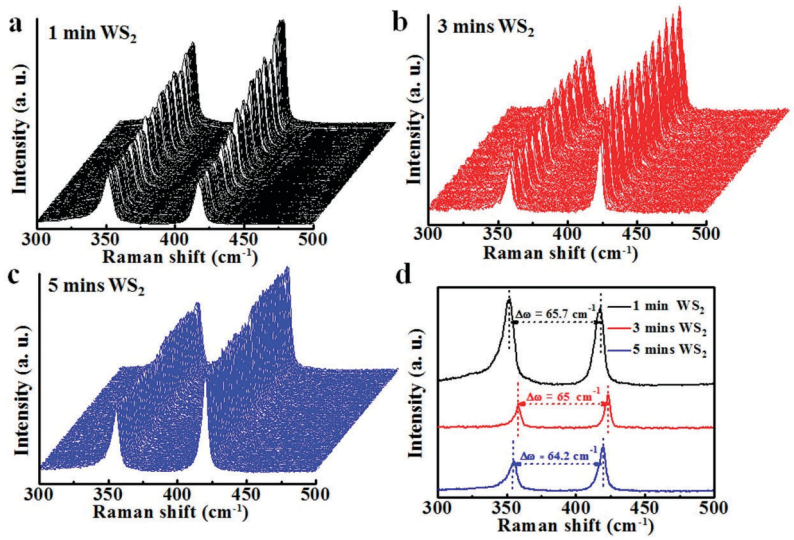

Fig. 3 Raman spectra of WS_2 films extracted from the Raman mapping data obtained in 10 × 10 μm^2 regions of (a) 1 min, (b) 3 min and (c) 5 min WS_2 films. (d) Typical Raman spectra of WS_2 films showing the average frequency difference, $\Delta\omega$.

confirm that the 1 min WS_2 film contained a higher number of layers than the 3 and 5 min films. In conclusion, the layer numbers of WS_2 films fabricated with sputtering times of 3 min and 5 min are similar and are lower than the layer number of 1 min WS_2 film.

Transmission electron microscopy (TEM) was employed to characterize the layer number, crystallinity and structure of the WS_2 samples, as shown in Fig. 4(a, d and g) TEM and Fig. 4(b, e and h) high-resolution transmission electron microscopy (HRTEM) images. The energy-dispersive X-ray spectroscopy (EDS) spectra of three samples are shown in Fig. 4(c, f and i). These results showed that the 1 min WS_2 film consisted of large-area polycrystalline WS_2 film, but countless WS_2 nanosheets were found within the 3 min and 5 min WS_2 films. The results also showed that the 1 min and 3 min WS_2 sheets were mainly horizontally grown, while the 5 min films contained many vertically grown sheets, as shown in Fig. 4(g and h). The change in growth direction from horizontal to vertical is directly related to the amount of WS_2 deposited on the substrate – the thickness of the precursor WS_2 films. During post-annealing, sulfur vapor diffused into very thin amorphous WS_2 layers; the horizontal growth of large-area WS_2 was more energetically favorable than the growth of vertically aligned layers because WS_2 films with horizontal growth exposed low-surface-energy basal planes. However, when thick amorphous WS_2 films undergo post-annealing, horizontal volume expansion cannot be easily accommodated due to the precursor films anchored to the substrate. In this case, the horizontal growth of a large size and continuous film will produce a great deal of strain energy, and therefore, WS_2 films would grow vertically because of the unconstrained free volume expansion in the vertical direction.[58,59] Moreover, the HRTEM images in Fig. 3(b, e and h) show horizontally grown WS_2 sheets with 0.28 nm interplane spacing and vertically grown WS_2 sheets with layer spacing of 0.64 nm. The EDS spectra of the samples shown

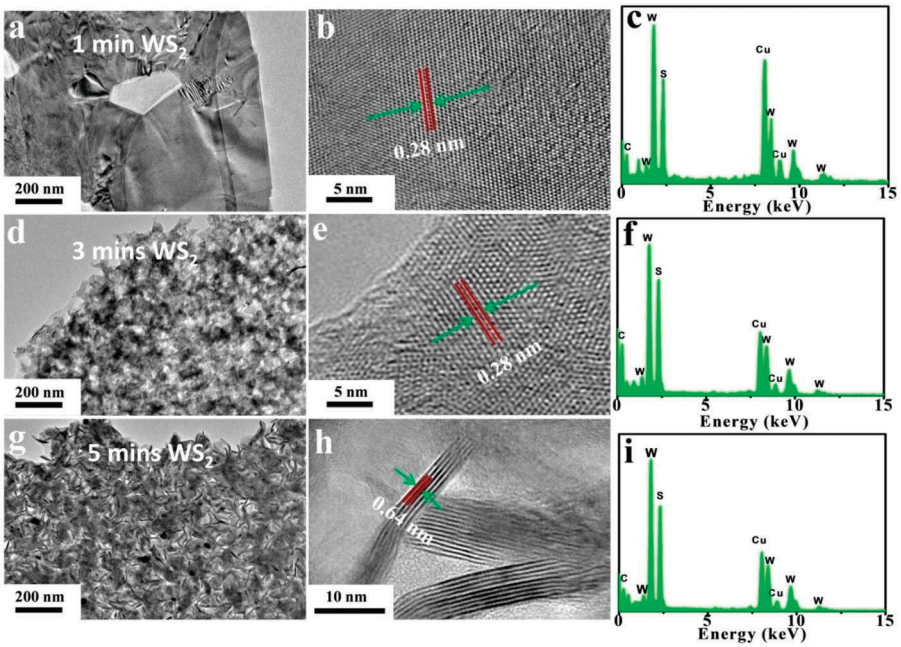

Fig. 4 Transmission electron microscopy (TEM) images of 1 min, 3 min and 5 min WS_2 films on carbon-coated copper fiber (a, d and g). Top view high-resolution transmission electron microscopy (HRTEM) images (b, e and h) of the vertically grown WS_2 nanosheets and the horizontally grown nanosheets. The lattice spacing was approximately 0.64 and 0.28 nm for vertically and horizontally grown WS_2 nanosheets, respectively. Energy-dispersive X-ray spectroscopy (EDS) spectra (c, f and i) of WS_2 films fabricated with different sputtering times (a–c, 1 min, d–f, 3 min, g–i, 5 min).

in Fig. 4(c, f and i) confirm that both the tungsten (W) and sulfur (S) from WS_2 were present in all the prepared samples. The detected carbon (C) and copper (Cu) were from the carbon-coated copper substrate used for the TEM measurement.

Cross-sectional TEM images of the three samples were taken for further investigation of the internal structure of the WS_2 films and are shown in Fig. 5. The cross-sectional TEM images of WS_2 films with different thicknesses are shown in Fig. 5(a–c). The WS_2 films deposited with 1 min, 3 min and 5 min sputtering times had uniform thicknesses of approximately 11, 15, and 30 nm, and the numbers of layers estimated from the above cross-sectional TEM images were approximately 18–20, 15–17 and 8–10, respectively. When the sputtering time was increased from 1 min to 3 min, vertically grown nanosheets began to appear. In the sample fabricated with a 5 min deposition time, a large number of vertically grown nanosheets were clearly produced.

To investigate the exciton dynamics of the few-layer WS_2 films, the exciton radiative lifetime of a WS_2 film was measured by using an 800 nm (100 fs) excitation laser source. Fig. 6 presents the decay curve for the 5 min WS_2 film on a linear scale and a logarithmic scale. The decay curve clearly exhibits multi-exponential decay and can be well fitted using the triple exponential decay function $A_1e^{-t/\tau_1} + A_2e^{-t/\tau_2} + A_3e^{-t/\tau_3}$, where $\tau_1 < \tau_2 < \tau_3$; τ_i denotes the exponential decay lifetime of each component in the WS_2 nanofilms; each pre-exponential factor A_i is the corresponding weight of the i'th component; and the subscript i is equal to 1, 2 or 3. The fitting decay time constants are τ_1 = 512 ps (67.5% of weight), τ_2 = 1311 ps (26.2% of weight)

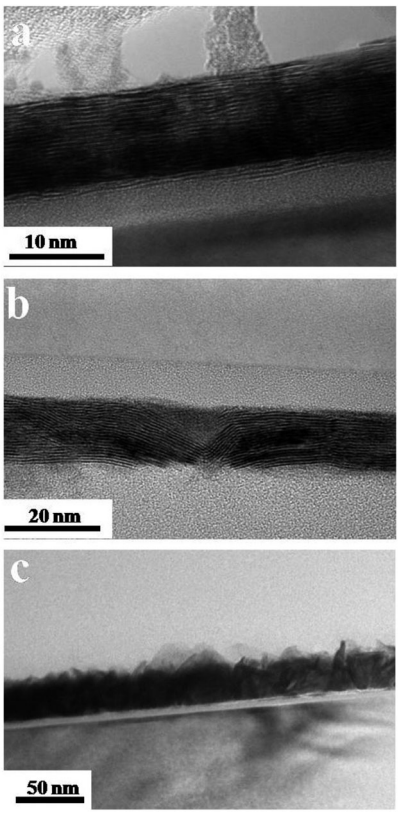

Fig. 5 Cross-sectional HRTEM images of the WS_2 films. (a) 1 min, (b) 3 min and (c) 5 min.

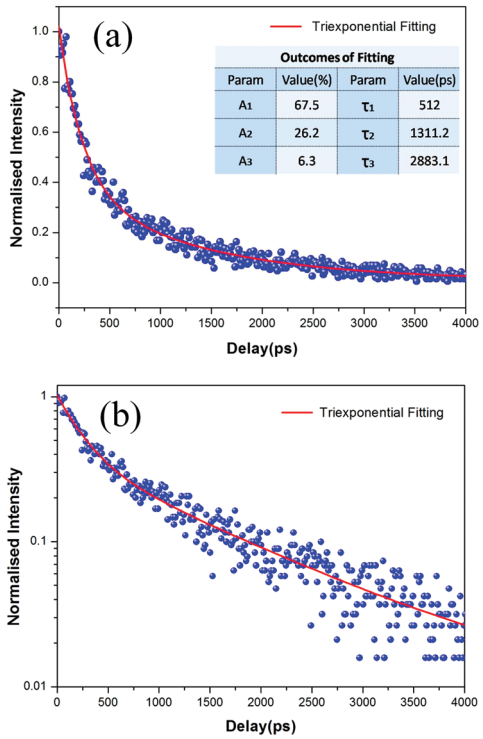

Fig. 6 Exciton dynamics for 5 min WS_2 film with a pump wavelength of 800 nm on a linear scale (a) and a logarithmic scale (b), revealing multi-exponential decay. The solid line is fitted using a triexponential decay function, and the outcomes of the fitting are presented in the inset table.

and τ_3 = 2883 ps (6.3% of weight). Thus, the corresponding mean decay time (τ_m) of the WS_2 film is 870.71 ps. This result is essentially consistent with the decay time of WS_2 nanosheets ($\sim$1 ns) presented in previous research works.[60,61]

3 Experimental results

Two sets of Z-scan experimental data are presented to examine the relationship between the nonlinear optical (NLO) properties of WS_2 samples fabricated with different sputtering times (1 min, 3 min and 5 min) under condition (A), a constant pulse width (100 fs) but varying pump pulse energies (1 μJ, 1.5 μJ and 2 μJ), and condition (B), a constant pump pulse energy (2 μJ) but varying pulse durations (100 fs, 200 ps, 10 ps and 10 ns). The Ti-sapphire excitation laser source was operated at 800 nm for all the experiments. A schematic diagram of the experimental setup of the open aperture Z-scan is shown in the ESI:† Fig. S1. The Z-scan experimental data marked with squares, circles, triangles and rhombuses are shown in Fig. 7 and 8, and all the related theoretical fittings shown by solid lines were calculated by eqn (2).

3.1 Condition (A) a constant pulse width (100 fs) but various pump pulse energies (1 μJ, 1.5 μJ and 2 μJ)

Only SA was observed for all samples under excitation by a 100 fs pulse with various pulse energies, as shown in Fig. 7. The NLO effect grew stronger as the pulse energy increased.

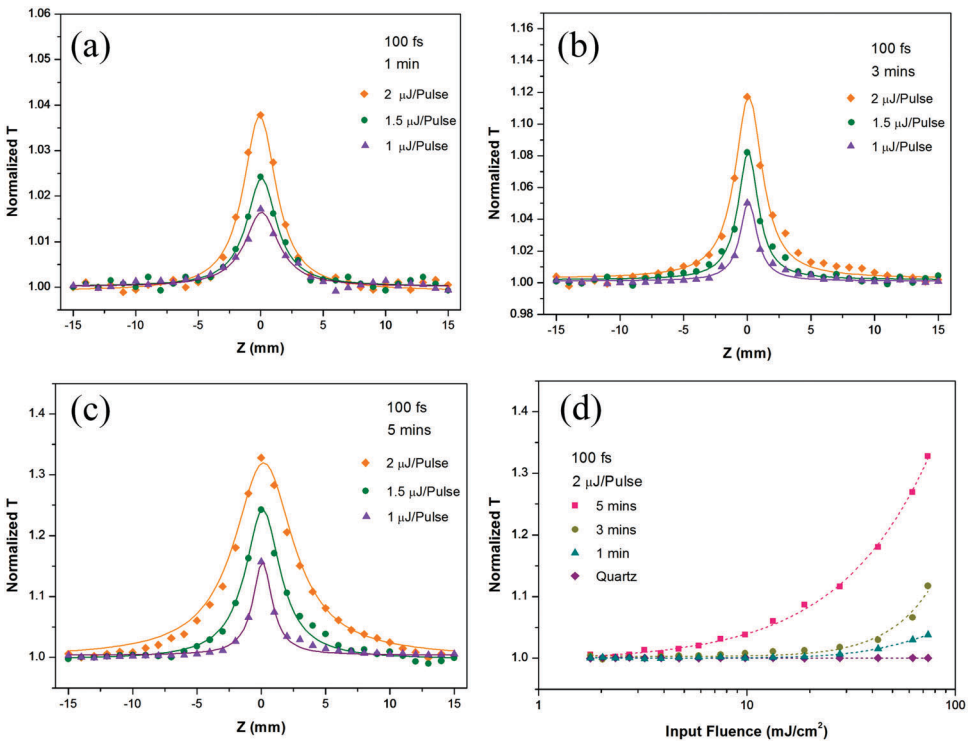

Fig. 7 Open aperture Z-scan results for few-layer WS_2 films fabricated with different magnetron sputtering times (a, 1 min; b, 3 min; c, 5 min) at a 100 fs (800 nm) laser pulse with different energies. (d) Normalized transmittance *versus* input fluence for 1 min, 3 min, and 5 min WS_2 films and the pure quartz substrate under 2 μJ laser pulse excitation.

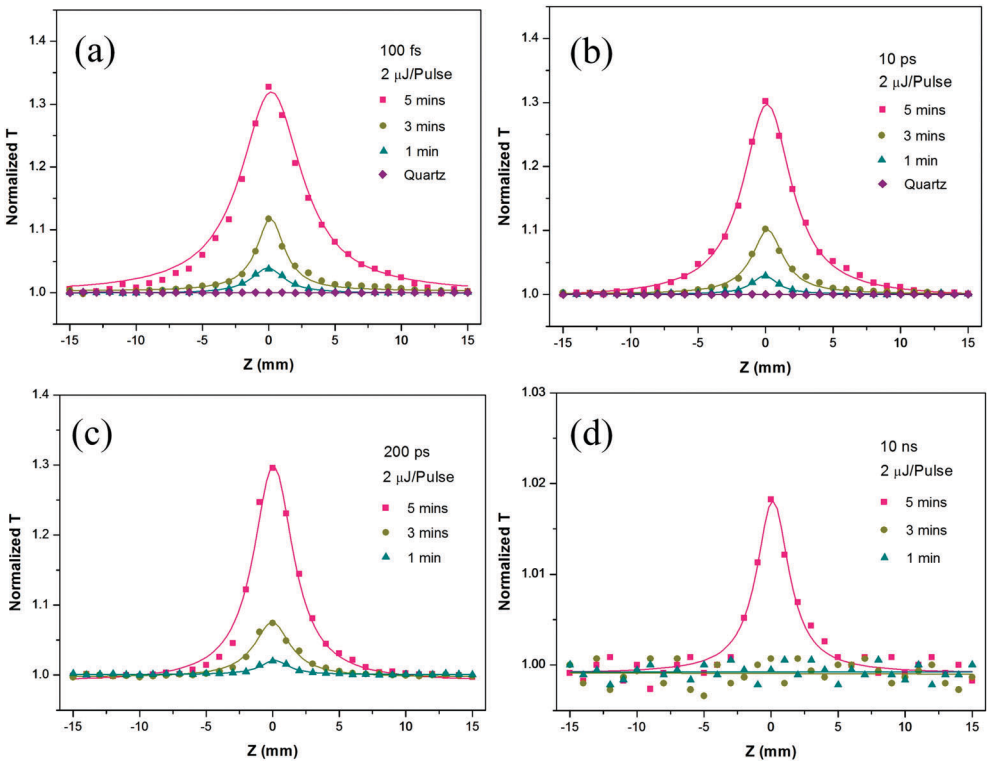

Fig. 8 Z-scan results of 1 min, 3 min and 5 min WS_2 films for (a) 100 fs, (b) 10 ps, (c) 200 ps and (d) 10 ns laser pulses at 800 nm. The response for the pure substrate is also included.

The measured normalized transmission increased to its maximum as the sample position approached the focus. The Z position shown in Fig. 7(a)–(c) can be translated into input fluence, which can be calculated by dividing the input pulse energy by the measured beam spot area at different Z positions. An example is given in Fig. 7(d), which shows the normalized transmission with respect to different input fluences under excitation by a 2 μJ 100 fs pulse. No NLO effect was observed from the quartz substrate alone. Therefore, the NLO properties were derived from the deposited WS_2 materials. These results indicate that the 5 min sample with the larger pulse energy (2 μJ) exhibited the strongest SA properties among the various samples and excitation pulse energies. The observed results are reasonable, as the SA effect depends on the amount of nonlinear materials and the pulse energy. To ensure the NLO properties were not the results of nonlinear optical damage, the sample was examined under a microscope after each experiment. No laser damage was observed for all samples under excitation by a pulse energy of 2 μJ.

3.2 Condition (B) the same pump pulse energy (2 μJ) but various pulse duration (100 fs, 200 ps, 10 ps and 10 ns)

This section presents the experimental data for various WS_2 film samples under excitation by the same pulse energy 2 μJ with different pulse widths. This information will give us a deeper understanding of the NLO properties of these materials changes with respect to pulse width modulation.

As shown in Fig. 7 and 8, all the samples exhibited a prominent ultrafast SA response or no NLO response. The SA behaviors observed for the three WS_2 films implied that their band gap energies were all smaller than 1.55 eV (the one-photon energy of the 800 nm exciting laser). The band gap of the few-layer WS_2 films was approximately 1.3 eV based on the previous reports.[33,62,63] Therefore, the NLO effects of the three WS2 nanofilms can be attributed to the strong single photon absorption and Pauli blocking in semiconductor materials.[64]

4 Nonlinear absorption model and discussion

The following nonlinear absorption model was widely used to fit all the Z-scan data and to quantitatively analyze the corresponding NLO coefficients:[65,66]

$$\alpha(I) = \alpha_0 - \alpha_{NL} I \quad (1)$$

where $\alpha(I) = -dI/(I \cdot dz')$ is the total absorption coefficient, including the linear absorption term α_0 and the nonlinear absorption coefficient α_{NL}; $I = I(z')$ is the intensity distribution within the sample; and z' is the propagation length within the sample. We can solve eqn (1) exactly and obtain the normalized power transmission as follows:

$$T(z) = \frac{\ln[1 + q_0(z)]}{q_0(z)} \quad (2)$$

Table 1 Optical parameters of linear transmittance (T_L), linear absorption coefficient (α_0), nonlinear absorption coefficient (α_{NL}), saturation irradiance (I_S), NLO onset fluence (F_{on}), and NLO modulation depth (ΔT) for few-layer WS_2 films. The calculation details of the different parameters are given in the ESI

Sample	800 nm laser	T_L (%)	α_0 (cm^{-1})	α_{NL} (cm GW^{-1})	I_S (GW cm^{-2})	F_{on} (mJ cm^{-2})	ΔT (%)
1 min WS_2	100 fs	94.84	6.97×10^4	97.55 ± 8.83	306.16 ± 25.41	18.86	3.8
	10 ps			$(9.63 \pm 0.18) \times 10^3$	3.1 ± 0.06	27.9	2.9
	200 ps			$(1.66 \pm 0.33) \times 10^5$	0.18 ± 0.03	42.5	1.9
3 min WS_2	100 fs	79.25	1.58×10^5	162.96 ± 15.70	455.07 ± 39.99	7.47	11.7
	10 ps			$(1.67 \pm 0.02) \times 10^4$	4.45 ± 0.05	9.8	10.2
	200 ps			$(2.77 \pm 0.40) \times 10^5$	0.27 ± 0.03	13.32	7.4
5 min WS_2	100 fs	60.97	1.91×10^5	314.67 ± 5.43	282.63 ± 4.8	2.73	32.1
	10 ps			$(2.87 \pm 0.01) \times 10^4$	3.09 ± 0.01	3.87	30.2
	200 ps			$(5.71 \pm 0.40) \times 10^5$	0.16 ± 0.01	5.86	28.5
	10 ns			$(2.20 \pm 0.42) \times 10^6$	0.04 ± 0.006	42.5	1.8

where $q_0(z) = \alpha_{NL} I_0 L_{eff}/(1 + z^2/{z_0}^2)$, $L_{eff} = (1 - e^{-\alpha_0 L})/\alpha_0$; I_0 is the on-axis intensity at the focus of the beam (*i.e.*, $z = 0$); and z_0 is the beam diffraction length. The linear transmittance (T_L) and absorption coefficient (α_0) of the WS_2 films were measured and are given in Table 1. The reflectance of the quartz substrate of the sample has been taken into account in the measurement. Then, eqn (2) was used to generate the solid fitting lines for the Z-scan experimental data shown in Fig. 7 and 8. The fitting lines agree well with the measured Z-scan experimental data. The measurement precision was improved by averaging ten measurements. For the 100 fs laser pulses, the corresponding fitted α_{NL} values used for the 1 min, 3 min and 5 min WS_2 films were approximately 97.55 cm GW^{-1}, 162.96 cm GW^{-1} and 314.67 cm GW^{-1}, respectively, as given in Table 1. The increasing values of α_{NL} indicate that the NLO absorption increases continuously for samples with longer sputtering times. The saturation intensity I_s is also widely adopted to evaluate the performance of SA materials and is critical for evaluating the pulse-shortening effect in the pulse generation. I_s is generally defined by $\alpha(I) = \alpha_0/(1 + I/I_s)$, which means that the absorption coefficient $\alpha(I)$ will be reduced to half of its original value α_0 for the incident intensity $I = I_s$. By setting $\alpha(I) = \alpha_0/2$ in eqn (1), we obtain $I_s = \alpha_0/(2\alpha_{NL})$, and then the values of I_s for the WS_2 films with 100 fs pulses can be calculated and are shown in Table 1. In contrast to the other SA nanomaterials presented in previous works with 800 nm (100 fs) pulses, *e.g.*, TMD dispersions or films,[67,68] graphene oxide (GO) films[69] and graphene,[29,70,71] the 5 min WS_2 film exhibited relatively low I_s values of 282.63 GW cm^{-2}.

Table 1 shows that the linear transmittance, T_L, decreases and the linear absorption coefficient, α_0, increases with the sputtering time as more WS_2 is deposited on the substrate. The value of α_{NL} also increases with sputtering time. This result implies that the nonlinear absorption will increase with increasing deposition time. For instance, α_{NL} of the 5 min film is approximately three times higher than that of the 1 min film for 100 fs, 10 ps and 200 ps pulses. However, I_s of all the three WS_2 films did not change greatly with respect to sputtering time but decreased rapidly for increasing pulse duration, *e.g.*, I_s of the 5 min sample decreased from 282.63 GW cm^{-2} for 100 fs to 0.16 GW cm^{-2} for 200 ps, which, to the best of our knowledge, is the lowest I_s among TMDs in the ps region.[29,66,68]

The onset fluence (F_{on}) denotes the NLO onset threshold, defined as the input fluence point at which the normalized transmittance of SA materials begins to increase. The modulation depth (ΔT) is the maximum possible change in transmittance induced by incident laser pulses. F_{on} and ΔT are two important SA parameters which are widely used to evaluate the practical performance of saturable absorbers. In general, for a saturable absorber used in passive mode-locking or Q-switching lasers, a lower F_{on} means lower laser threshold for the onset of pulse operation and a larger ΔT leads to shorter pulse generation and more reliable self-starting of mode-locking.[50–53] For easy comparison, the onset fluence F_{on} and modulation depth ΔT are plotted against the sputtering times of samples for different pulse width at the same excitation energy of 2 μJ in Fig. 9(a and b) respectively. As shown in Fig. 9 and Table 1, generally, as the magnetron sputtering time increased from 1 min to 5 min, the onset fluence F_{on} of the SA response dropped, and the modulation depth ΔT of SA increased. This indicates that F_{on} decreases and ΔT increases with increasing film thickness, decreasing numbers of layers, and increasing amount of vertically grown WS2 nanosheet. For various pulse duration, the key SA parameters, modulation depth ΔT and onset fluence F_{on}, have been demonstrated to be greatly modifiable by controlling the film thickness and structure *via* adjusting the magnetron sputtering time during the fabrication process.

In this section, the modulation of F_{on} and ΔT by changing the sputtering time at various pulse widths will be discussed. Generally, the modulation of F_{on} and ΔT is quite large: (1) F_{on} was reduced by ~86% for all three pulse durations (100 fs, 10 ps and 200 ps). (2) The value of ΔT was also greatly enhanced by 840%, 1040% and 1500% for 100 fs, 10 ps and 200 ps pulses. These enhancements were achieved by increasing the sputtering time from 1 min to 5 min. Therefore, we can conclude that the values of F_{on} and ΔT can be modified greatly by changing the sputtering time. Compared with other WS_2 films used in previous studies under the same excitation wavelength and duration of 800 nm and 100 fs, respectively, the WS_2 films used in this work exhibited larger modulation depth ΔT. With a similar value of $T_L \approx 95\%$, the ΔT value obtained for the 1 min sample was 3.8%, which was approximately 50% larger than the previous record.[67]

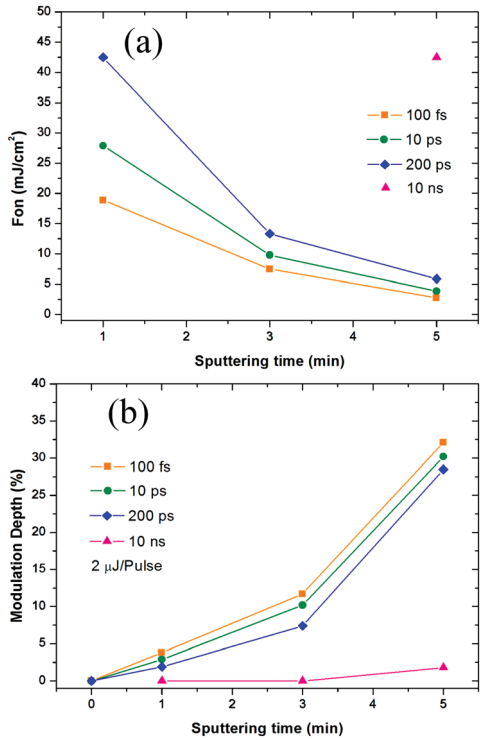

Fig. 9 Onset fluence F_{on} (a) and modulation depth ΔT (b) of WS_2 films fabricated with different sputtering times for 100 fs, 10 ps, 200 ps and 10 ns laser pulses (800 nm, 2 μJ).

Additionally, Fig. 9 and Table 1 reveal that the changes in F_{on} and ΔT with respect to the changing pulse width can also be quantified. F_{on} approximately doubled (~100%) for all three samples as the pulse duration was changed from 100 fs to 200 ps (1000 times). The value of ΔT decreased by 50% for the 1 min, 36.7% for the 3 min and 11.2% for the 5 min sample as the pulse width increased from 100 fs to 200 ps. The reduction in ΔT was smaller for WS_2 samples with longer sputtering times. Fig. 8(d) and 9 show weak SA for the 5 min sample under the excitation of a 10 ns pulse and no SA for the other two samples. For this reason, only a single data point for the 10 ns pulse is shown in Fig. 9(a and b). Overall, the WS_2 films prepared for this work possess prominent ultrafast SA parameters in both the fs and ps regions and can fully satisfy various ultrafast SA device applications, including passive mode-lockers, passive Q-switchers, optical switches, *etc.* These results confirm that the 5 min sample offers the strongest NLO properties, and therefore, Fig. 10(a–c) were plotted for the detailed comparison of various pulse widths.

Fig. 10 summarizes the SA responses of the 5 min sample. The SA of the sample decayed slowly when the pulse width increased from fs to ps but was sharply weakened by the ns pulse excitation, as shown in Fig. 10(a)–(c). The corresponding pulse width dependences of the SA modulation depth ΔT and the onset fluence F_{on} are shown in Fig. 10(c). Fig. 10(c) shows that ΔT decreased and F_{on} increased slowly when the pulse width was increased from 100 fs to 200 ps. However, the changes accelerated as the pulse width increased further from 200 ps to 10 ns. F_{on} increased dramatically from 5.86 mJ cm^{-2} to 42.5 mJ cm^{-2} (725%) as the pulse duration changed from 200 ps to 10 ns. A dramatic reduction from 28.5% to 1.8% (1583%) in ΔT of the 5 min WS_2 sample occurred as the pulse duration changed from 200 ps to 10 ns. Notably, as the duration of the laser pulses increased from 100 fs to 200 ps, the peak power of the laser pulses decreased by 2000 times, but the values of ΔT and F_{on} showed no obvious changes. As far as we know, no interpretation or theoretical analysis of this phenomenon exists. The mechanism by which the SA parameters of such TMDs varied with the pulse width thus far remains unclear.

In this section, a pulse width-dependent SA theoretical model that considers the effects of the interband exciton recombination is first proposed to understand and analyze the mechanism by which the SA properties of WS_2 vary with the excitation pulse width. Then, two analytical expressions for the key SA parameters (F_{on} and ΔT) in term of pulse width are deduced by using the energy band theory and exciton dynamics of the WS_2 nanofilms. As shown in Fig. 10(d), a large number of free carriers are excited from the valence band to level C of the conduction band. These photoexcited electrons consequently decay to lower energy levels by intraband relaxation (<500 fs).[60,72] When the input fluence is greater than or equal to the SA onset fluence F_{on}, the states below the energy level C in the conduction band are fully filled. Then, further absorption is blocked (*i.e.*, Pauli-blocking), and saturated absorption occurs.[73] Interband charge recombination has usually been ignored in previous research works.[29,67,68] In fact, the excitons at the bottom of the conduction band relax by interband recombination at the speed $1/\tau$, where τ is the exciton radiative decay lifetime of the material. However, within the pump pulse duration, the decayed electrons reabsorb another photon and jump back into the conduction band to refill the unfilled states. This process is dynamic. The ratio between pulse duration, t, and the exciton radiative decay lifetime plays a critical role in SA properties. The exciton radiative decay is generally believed to be negligible if it is much longer than the pump pulse duration. However, as mentioned previously, decay will always occur even within the exciton decay lifetime. Based on our experimental data shown in Table 1, even within the decay lifetime (~0.87 ns), a longer excitation pump pulse (200 ps) will still exhibit a higher F_{on} than that of 100 fs, although by only 2 times. However, if the pulse width is much longer than the decay lifetime, F_{on} is expected to become much higher as the exciton decay becomes more significant. Thus, if the sample is pumped within its lifetime, energy can be efficiently absorbed for the SA effect. The duration of the 10 ns pulse is much longer than the WS_2 decay lifetime, which implies that the decay of excited electrons becomes significant and that, therefore, more pumping energy is needed to saturate the sample. Accordingly, the following new theoretical model based on the ratio of t and τ was developed to account for interband recombination.

During this process, the maximum excited state population, N_{on}, was kept constant, and then the total number of the recombination excitons, ΔN, could be calculated by

$$\Delta N = N_{on} \cdot \frac{t}{\tau} \quad (3)$$

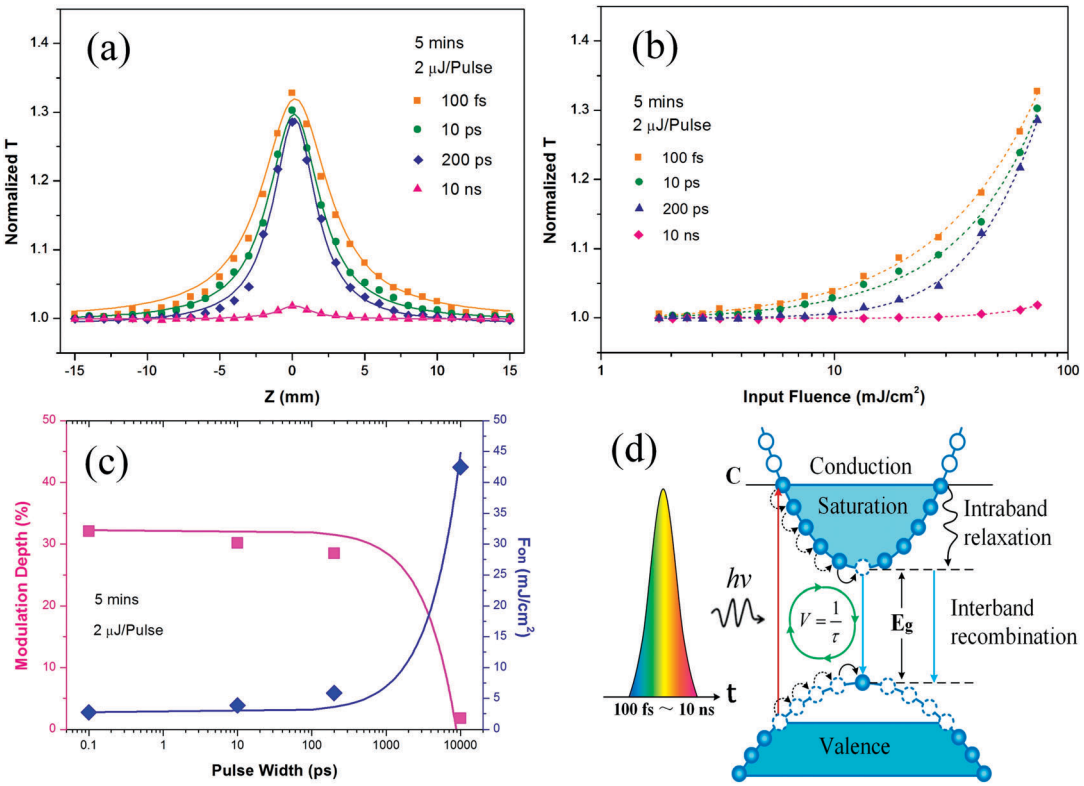

Fig. 10 Comparison of SA responses (normalized transmittance *versus Z* position (a) and input fluence (b)) of the 5 min WS_2 film for 100 fs, 10 ps, 200 ps and 10 ns laser pulses with 2 μJ energy. (c) Corresponding SA modulation depth ΔT and onset fluence F_{on} as a function of excitation pulse width. The solid curves were plotted to show the conclusions of our theoretical model. Square – modulation depth; diamond – F_{on}. (d) Schematic of SA and relaxation processes in WS_2 film excited by ultrashort laser pulses.

For the exciton dynamics described above, $1/\tau$ is the interband recombination speed of the WS_2 nanofilms, and $1/\tau = A_1 \cdot 1/\tau_1 + A_2 \cdot 1/\tau_2 + A_3 \cdot 1/\tau_3$; τ_i denotes the exponential decay lifetime of each component in the WS_2 nanofilms; and A_i denotes the corresponding weights. The subscript i can equal 1, 2 or 3. After a few steps (the detailed derivation is given in the ESI†), eqn (4) and (5) can be obtained:

$$F_{on} \approx F_{on}{}' \left(1 + \frac{t}{\tau}\right) \tag{4}$$

and

$$\Delta T \approx \Delta T' - \frac{(1 - T_L)F_{on}{}'}{T_L F_0} \cdot \frac{t}{\tau}, \tag{5}$$

where F_{on} and ΔT represent the onset fluence and modulation depth, respectively. F_0 is the laser fluence at $z = 0$, and $F_{on}{}'$ and $\Delta T'$ are the values of F_{on} and ΔT for the pulse width $t = 100$ fs. The analytical expressions (4) and (5) show the regular variation of the SA parameters F_{on} and ΔT with the excitation pulse width t. For the 5 min WS_2 film, $T_L = 60.97\%$, $a = 0.3903$, $F_{on}{}' = 2.73$ mJ cm^{-2}, $F_0 = 73.9$ mJ cm^{-2}, $T_0{}' = 80.54\%$, $A_1 = 67.5\%$, $\tau_1 = 512$ ps, $A_2 = 26.2\%$, $\tau_2 = 1311$ ps, $A_3 = 6.3\%$, and $\tau_3 = 2883$ ps. Substituting these parameters into eqn (4) and (5) produces the two solid curves shown in Fig. 10(c) to describe the relationship between the key parameters (F_{on}, ΔT) and the pulse duration, t, for the 5 min WS_2 sample. Both theoretical curves agree well with the experimental data. Thus, the dramatic change of the SA properties of these samples in the fs, ps and ns regions can be well described by the SA theoretical model and analytical expressions developed here. Overall, the newly developed theoretical model and the experimental data confirmed that the SA parameters of these WS_2 films can be modified by controlling the sputtering time. These research findings are vital for the design and engineering of TMD-based nonlinear materials for various applications, *e.g.*, ultrafast lasers, nanosecond lasers, ultrafast pulse shaping, optical switching, optical communications, and optical computing.

5 Conclusions

In summary, large-area samples of WS_2 nanofilms with different thicknesses and morphologies deposited on quartz were fabricated by magnetron sputtering for various deposition times. The 1 min and 3 min WS_2 films contained mainly horizontally grown WS_2, while the 5 min films contained many vertically grown few-layered WS_2 nanosheets. The characteristics and the ultrafast NLO properties of these nanofilms were investigated systematically by Z-scan. The WS_2 films were found to possess prominent ultrafast SA properties under excitation by an 800 nm pulsed laser with energy up to 2 μJ and varying pulse durations in the fs, ps and ns regions. Some key SA parameters, *e.g.*, the onset fluence F_{on} and

the modulation depth ΔT, can be greatly modified by adjusting the thickness and morphology *via* controlling the magnetron sputtering time. A pulse width-dependent SA model that considers the effects of interband exciton recombination was proposed for the first time. The ratio between the decay lifetime and pulse width is critical for the SA effect. Laser pulses with the same pulse energy but a duration shorter than the decay lifetime produce a stronger SA effect. Two analytical expressions for the variation of the onset fluence F_{on} and the modulation depth ΔT with the excitation laser pulse width are derived. Our experimental results were in good agreement with the analytical predictions. These expressions can be employed to calculate the values of F_{on} and ΔT for various pulse widths for the TMD materials and further develop various ultrafast lasers and nanosecond lasers. These research findings have great value for both basic science and practical applications.

Conflicts of interest

There are no conflicts to declare.

Acknowledgements

We would like to thank Associate Professor Wei Zheng from the Shenzhen Institutes of Advanced Technology, Chinese Academy of Sciences for measuring the decay lifetimes of the WS_2 nanofilms. This work is financially supported by the Shenzhen-Hong Kong Innovation Cooperation Project (Grant No. SGLH20150205162842428), Hong Kong Innovation and technology fund under Grant GHP/007/14SZ, the Research Grants Council of Hong Kong, China (Project Number: GRF 152109/16E PolyU B-Q52T), the Science and Technology Innovation Commission of Shenzhen (JCYJ20170412111625378, JCYJ20170302153540973 and GRCK2017042110412823), the National Special Foundation of China for Major Science Instrument (61227802) and Hong Kong Polytechnic University (Project number: G-YBFR).

Notes and references

1 F. Xia, H. Wang, D. Xiao, M. Dubey and A. Ramasubramaniam, *Nat. Photonics*, 2014, **8**, 899–907.
2 A. K. Geim, *Nat. Mater.*, 2007, **6**, 183–190.
3 A. K. Geim, *Science*, 2009, **324**, 1530–1534.
4 L. H. Zeng, M. Z. Wang, H. Hu, B. Nie, Y. Q. Yu, C. Y. Wu, L. Wang, J. G. Hu, C. Xie and F. X. Liang, *ACS Appl. Mater. Interfaces*, 2013, **5**, 9362–9366.
5 L. Zeng, C. Xie, L. Tao, H. Long, C. Tang, Y. H. Tsang and J. Jie, *Opt. Express*, 2015, **23**, 4839–4846.
6 B. Nie, J. G. Hu, L. B. Luo, C. Xie, L. H. Zeng, P. Lv, F. Z. Li, J. S. Jie, M. Feng and C. Y. Wu, *Small*, 2013, **9**, 2872–2879.
7 W. Y. Kong, G. A. Wu, K. Y. Wang, T. F. Zhang, Y. F. Zou, D. D. Wang and L. B. Luo, *Adv. Mater.*, 2016, **28**, 10725–10731.
8 L. B. Luo, J. J. Chen, M. Z. Wang, H. Hu, C. Y. Wu, Q. Li, L. Wang, J. A. Huang and F. X. Liang, *Adv. Funct. Mater.*, 2014, **24**, 2794–2800.
9 Y. Ye, G. Lin, L. Dai, M. Hu, W. Feng, D. Yu, Z. Shi, B. Yu, X. Guo and G. Qin, *J. Mater. Chem.*, 2011, **21**, 11760–11763.
10 Y. M. Lin, C. Dimitrakopoulos, K. A. Jenkins, D. B. Farmer, H. Y. Chiu, A. Grill and P. Avouris, *Science*, 2010, **327**, 662.
11 Z. Li, W. Xu, Y. Yu, H. Du, K. Zhen, J. Wang, L. Luo, H. Qiu and X. Yang, *J. Mater. Chem. C*, 2015, **4**, 362–370.
12 L. B. Luo, C. Xie, X. H. Wang, Y. Q. Yu, C. Y. Wu, H. Hu, K. Y. Zhou, X. W. Zhang and J. S. Jie, *Nano Energy*, 2014, **9**, 112–120.
13 C. Meng, S. L. Yu, H. Q. Wang, Y. Cao, L. M. Tong, W. T. Liu and Y. R. Shen, *Light: Sci. Appl.*, 2015, **4**, e348.
14 Y. Wang, Z. S. Qu, J. Liu and Y. H. Tsang, *J. Light Technol.*, 2012, **30**, 3259–3262.
15 D. Jariwala, T. J. Marks and M. C. Hersam, *Nat. Mater.*, 2017, **16**, 170.
16 J. Yang, R. Xu, J. Pei, W. M. Ye, F. Wang, Z. Wang, S. Zhang, Z. Yu and Y. Lu, *Light: Sci. Appl.*, 2015, **4**, e312.
17 J. Xiao, Z. Ye, Y. Wang, H. Zhu, Y. Wang and X. Zhang, *Light: Sci. Appl.*, 2015, **4**, 366.
18 L. Zhu, F. Liu, H. Lin, J. Hu, Z. Yu, X. Wang and S. Fan, *Light: Sci. Appl.*, 2016, **5**, e16052.
19 K. F. Mak and J. Shan, *Nat. Photonics*, 2016, **10**, 216–226.
20 Y. Shi, H. Li and L. J. Li, *Chem. Soc. Rev.*, 2015, **44**, 2744–2756.
21 L. Zeng, L. Tao, C. Tang, B. Zhou, H. Long, Y. Chai, S. P. Lau and Y. H. Tsang, *Sci. Rep.*, 2016, **6**, 20343.
22 M. L. Tsai, S. H. Su, J. K. Chang, D. S. Tsai, C. H. Chen, C. Wu, L. J. Li, L. J. Chen and J. H. He, *ACS Nano*, 2014, **8**, 8317.
23 L. H. Zeng, S. H. Lin, Z. J. Li, Z. X. Zhang, T. F. Zhang, C. Xie, C. H. Mak, Y. Chai, S. P. Lau, L. B. Luo and Y. H. Tsang, *Adv. Funct. Mater.*, 2018, DOI: 10.1002/adfm.201705970.
24 H. Long, L. Tao, C. Y. Tang, B. Zhou, Y. Zhao, L. Zeng, S. F. Yu, S. P. Lau, Y. Chai and Y. H. Tsang, *Nanoscale*, 2015, **7**, 17771–17777.
25 L. Tao, H. Long, B. Zhou, S. F. Yu, S. P. Lau, Y. Chai, K. H. Fung, Y. H. Tsang, J. Yao and D. Xu, *Nanoscale*, 2014, **6**, 9713–9719.
26 H. Long, L. Tao, C. Y. Tang, H. Y. Tam, Q. Wen and Y. H. Tsang, *J. Mater. Chem. C*, 2016, **4**, 678–683.
27 C. Chen, W. Yu, T. Liu, S. Cao and Y. Tsang, *Sol. Energy Mater. Sol. Cells*, 2017, **160**, 43–53.
28 J. Zhou, S. Dai, W. Dong, X. Su, L. Fang, F. Zheng, X. Wang and M. Shen, *Appl. Phys. Lett.*, 2016, **109**, 332.
29 K. Wang, J. Wang, J. Fan, M. Lotya, A. O'Neill, D. Fox, Y. Feng, X. Zhang, B. Jiang and Q. Zhao, *ACS Nano*, 2013, **7**, 9260.
30 W. Shuxian, Y. Haohai, Z. Huaijin, W. Aizhu, Z. Mingwen, C. Yanxue, M. Liangmo and W. Jiyang, *Adv. Mater.*, 2014, **26**, 3538.
31 H. Zhang, S. B. Lu, J. Zheng, J. Du, S. C. Wen, D. Y. Tang and K. P. Loh, *Opt. Express*, 2014, **22**, 7249–7260.
32 K. Wu, X. Zhang, J. Wang, X. Li and J. Chen, *Opt. Express*, 2015, **23**, 11453–11461.

33 W. Zhao, Z. Ghorannevis, L. Chu, M. Toh, C. Kloc, P. H. Tan and G. Eda, *ACS Nano*, 2012, **7**, 791–797.
34 C. Y. Tang, P. K. Cheng, L. Tao, H. Long, L. H. Zeng, Q. Wen and Y. H. Tsang, *J. Light Technol.*, 2017, 1.
35 P. Yan, H. Chen, A. Liu, K. Li, S. Ruan, J. Ding, X. Qiu and T. Guo, *IEEE J. Sel. Top. Quantum Electron.*, 2016, **23**, 33–38.
36 Y. Cheng, J. Peng, B. Xu, H. Yang, Z. Luo, H. Xu, Z. Cai and J. Weng, *IEEE Photonics J.*, 2017, **8**, 1–6.
37 Z. Luo, D. Wu, B. Xu, H. Xu, Z. Cai, J. Peng, J. Weng, S. Xu, C. Zhu and F. Wang, *Nanoscale*, 2016, **8**, 1066.
38 W. Li, J. Peng, Y. Zhong, D. Wu, H. Lin, Y. Cheng, Z. Luo, J. Weng, H. Xu and Z. Cai, *Opt. Mater. Express*, 2016, **6**, 2031–2039.
39 M. Dong, Y. Wang, C. Ma, H. Lei, B. Jiang, X. Gan, S. Hua, W. Zhang, T. Mei and J. Zhao, *Sci. Rep.*, 2015, **5**, 7965.
40 C. Wei, H. Luo, H. Zhang, C. Li, J. Xie, J. Li and Y. Liu, *Laser Phys. Lett.*, 2016, **13**, 105108.
41 D. I. Yeom, H. Jeong, K. Oh, R. Khazaeinezhad, S. H. Kassani and T. Nazari, *Opt. Mater. Express*, 2015, **5**, 373–379.
42 D. I. Yeom, H. Jeong, K. Oh, R. Khazaeinezhad and S. H. Kassani, *J. Light Technol.*, 2015, **33**, 3550–3557.
43 L. Pang, W. Liu, W. Tian, H. Han and Z. Wei, *IEEE Photonics J.*, 2016, **8**, 1–7.
44 K. Y. Lau, A. A. Latif, M. H. A. Bakar, F. D. Muhammad, M. F. Omar and M. A. Mahdi, *Appl. Phys. B: Lasers Opt.*, 2017, **123**, 221.
45 B. Chen, X. Zhang, K. Wu, H. Wang, J. Wang and J. Chen, *Opt. Express*, 2015, **23**, 26723–26737.
46 P. Yan, A. Liu, Y. Chen, J. Wang, S. Ruan, H. Chen and J. Ding, *Sci. Rep.*, 2015, **5**, 12587.
47 B. Guo, Y. Yao, P. G. Yan, K. Xu, J. J. Liu, S. G. Wang and Y. Li, *IEEE Photonics Technol. Lett.*, 2016, **28**, 323–326.
48 C. Lan, C. Li, H. Xia, H. Li, S. Zhang, X. Zhang and Y. Liu, *Opt. Express*, 2014, **22**, 17341–17348.
49 A. Chernikov, C. Ruppert, H. M. Hill, A. F. Rigosi and T. F. Heinz, *Nat. Photonics*, 2015, **9**, 466–470.
50 F. X. Kurtner, J. A. D. Au and U. Keller, *IEEE J. Sel. Top. Quantum Electron.*, 1998, **4**, 159–168.
51 Q. W. Sheng, M. Feng, W. Xin, H. Guo, T. Y. Han, Y. G. Li, Y. G. Liu, F. Gao, F. Song and Z. B. Liu, *Appl. Phys. Lett.*, 2014, **105**, 666.
52 J. Li, H. Luo, Z. Bo, R. Lu, Z. Guo, Z. Han and L. Yong, *Sci. Rep.*, 2016, **6**, 30361.
53 C. Hönninger, R. Paschotta, F. Morier-Genoud, M. Moser and U. Keller, *J. Opt. Soc. Am. B*, 1999, **16**, 46–53.
54 B. Zhu, X. Chen and X. Cui, *Sci. Rep.*, 2015, **5**, 9218.
55 W. Zhao, Z. Ghorannevis, K. K. Amara, J. R. Pang, M. Toh, X. Zhang, C. Kloc, P. H. Tan and G. Eda, *Nanoscale*, 2013, **5**, 9677–9683.
56 A. Berkdemir, H. R. Gutiérrez, A. R. Botello-Méndez, N. Perea-López, A. L. Elías, C. I. Chia, B. Wang, V. H. Crespi, F. López-Urías and J. C. Charlier, *Sci. Rep.*, 2013, **3**, 1755.
57 H. Zeng, G. B. Liu, J. Dai, Y. Yan, B. Zhu, R. He, L. Xie, S. Xu, X. Chen and W. Yao, *Sci. Rep.*, 2013, **3**, 1608.
58 D. Kong, H. Wang, J. J. Cha, M. Pasta, K. J. Koski, J. Yao and Y. Cui, *Nano Lett.*, 2013, **13**, 1341.
59 Y. Jung, J. Shen, Y. Liu, J. M. Woods, Y. Sun and J. J. Cha, *Nano Lett.*, 2014, **14**, 6842–6849.
60 H. Shi, R. Yan, S. Bertolazzi, J. Brivio, B. Gao, A. Kis, D. Jena, H. G. Xing and L. Huang, *ACS Nano*, 2013, **7**, 1072–1080.
61 M. Palummo, M. Bernardi and J. C. Grossman, *Nano Lett.*, 2015, **15**, 2794.
62 D. Braga, I. G. Lezama, H. Berger and A. F. Morpurgo, *Nano Lett.*, 2012, **12**, 5218.
63 W. S. Yun, S. W. Han, S. C. Hong, I. G. Kim and J. D. Lee, *Phys. Rev. B: Condens. Matter Mater. Phys.*, 2012, **85**, 033305.
64 Q. Bao, Z. Han, W. Yu, Z. Ni, Y. Yan, Z. X. Shen, K. P. Loh and Y. T. Ding, *Adv. Funct. Mater.*, 2009, **19**, 3077–3083.
65 M. Sheik-Bahae, A. A. Said, T.-H. Wei, D. J. Hagan and E. W. Van Stryland, *IEEE J. Quantum Electron.*, 1990, **26**, 760–769.
66 M. Sheik-Bahae, A. A. Said and E. W. Van Stryland, *Opt. Lett.*, 1989, **14**, 955–957.
67 S. Zhang, N. Dong, N. Mcevoy, M. O'Brien, S. Winters, N. C. Berner, C. Yim, Y. Li, X. Zhang and Z. Chen, *ACS Nano*, 2015, **9**, 7142–7150.
68 K. Wang, Y. Feng, C. Chang, J. Zhan, C. Wang, Q. Zhao, J. N. Coleman, L. Zhang, W. J. Blau and J. Wang, *Nanoscale*, 2014, **6**, 10530–10535.
69 X. F. Jiang, L. Polavarapu, S. T. Neo, T. Venkatesan and Q. H. Xu, *J. Phys. Chem. Lett.*, 2012, **3**, 785.
70 P. L. Huang, W. L. Chen, T. W. Peng, C. Y. Su, C. Y. Yeh and W. H. Cheng, *IEEE Photonics Technol. Lett.*, 2015, **27**, 1791–1794.
71 S. Kumar, M. Anija, N. Kamaraju, K. S. Vasu, K. S. Subrahmanyam, A. K. Sood and C. N. R. Rao, *Appl. Phys. Lett.*, 2009, **95**, 183.
72 J. Shah, *Superlattices Microstruct.*, 1989, **6**, 293–302.
73 E. Garmire, *IEEE J. Sel. Top. Quantum Electron.*, 2002, **6**, 1094–1110.